Quantitative Bone Metastases Analysis Based on Image Segmentation

Yusuf E. Erdi, John L. Humm, Massimo Imbriaco, Henry Yeung and Steven M. Larson

Department of Medical Physics, Nuclear Medicine Service, Department of Radiology, Memorial Sloan-Kettering Cancer Center, New York, New York

Preliminary evidence indicates that the fraction of bone containing metastatic lesions is a strong prognostic indicator of survival longevity for prostate and breast cancer. Our current approach to quantify metastatic bone lesions, called the Bone Scan Index, is based on an inspection of the bone scan, estimating visually the fraction of each bone involved and then summing across all bones to determine the percentage of total skeletal involvement. This approach, however, is time consuming, subjective and dependent on individual interpretation. **Methods:** To overcome these problems, a semiautomated image segmentation program was developed for the quantitation of metastases from planar whole-body bone scans. The user is required to insert a seed point into each metastatic region on the image. The algorithm then connects pixels to the seed pixel in all directions until a contrast-dependent threshold is reached. The optimal threshold for cessation of the region growing is determined from phantom studies. On the images, lesion delineation and size measurements were performed by the algorithm. Each delineated lesion is associated with a bone site using pull-down menus. The program then computes the fraction of lesion involvement in each bone based on look-up-tables containing the relationship of bone mass with race, sex, height and age. These look-up-tables were obtained by multiple regression of the skeletal mass measurements in humans. The total fraction of skeletal involvement is then obtained from the individual fractional masses. For individual fractional mass, values given in International Commission on Radiation Protection Publication No. 23 were used. **Results:** The bone metastases analysis system has been used on 11 scans from 6 patients. The correlation was high (r = 0.83) between conventional (manually drawn region-of-interest) and this analysis system. Bone metastases analysis results in consistently lower estimates of fractional involvement in bone compared with the conventional region-of-interest drawing or visual estimation method. This is due to the apparent broadening of objects at and below the limits of resolution of the gamma camera. **Conclusion:** Image segmentation reduces the delineation and quantitation time of lesions by at least two compared with manual region-of-interest drawing. The objectivity of this technique allows the detection of small variations in follow-up patient scans for which the manual region-of-interest method may fail, due to performance variability of the user. This method preserves the diagnostic skills of the nuclear medicine physician to select which bony structures contain lesions, yet combines it with an objective delineation of the lesion.

Key Words: bone metastases; region growing; skeletal mass

J Nucl Med 1997; 38:1401–1406

More than 50% of patients with Hodgkin's disease or breast and prostate carcinoma have osseous metastases at autopsy (*1*). Similarly, other carcinomas frequently demonstrate osseous metastases ranging from 12% to 50% of cancer patients (*2*).

The fraction of bone containing metastatic lesions is a strong prognostic indicator of survival longevity for cancer (*3,4*). Especially in prostate cancer, the presence of bone metastases

outside of the pelvis and lumbar spine is a prognostic indicator of short survival time (*5*). However, to quantitate all bone metastases (BMets) in patients is a time-consuming task, since patients with metastatic involvement usually have more than one disease site. For example, one study identified 403 bone lesions in 62 patients (*6*). To evaluate and quantitate the fraction of metastatic deposits of BMets for such a group of patients may take up to 30 min per patient. In addition, the quantitation of skeletal disease is a subjective task based on the experience of the physician. To minimize the interobserver variability of the reading, usually more than one independent bone scan reader is used. In two recent studies, the extent of skeletal metastatic involvement was estimated as a percentage of the total skeletal area as independently determined by two bone scan readers (*7,8*). The values for each scan were then averaged for each observer to reduce the magnitude of interobserver variability.

Visual analysis of bone scans is a common method to estimate the extent of skeletal disease. In a recent study, the extent of skeletal disease was graded into five categories based on the number of bony metastases (*9*). Another study used a bone scan scoring system from 0 to 2, where 0 represents normal uptake, 1 means one or several uptakes and 2 signifies diffuse uptake (*10*). In a Mayo Clinic study, a similar bone scan interpretation schema was used as negative, positive or indeterminate (*11*).

Our current bone scan index (BSI) method is based on a subjective interpretation of the bone scan, in which the fraction of each bone involved is estimated visually. Each bone is then assigned to constitute a given fraction of the skeleton. By summing the fractional contribution of each bone, one arrives at the total percentage for the involved skeleton (*12*). This method uses the concept of standard man from International Commission on Radiation Protection (ICRP) Publication No. 23 (*13*), where 123 of the major bones in the body are listed by name, with their estimated fraction of the total skeleton. Physicians interpreting bone scans estimated the fraction of each involved bone by reference to an atlas. The sum of the involved area in the 123 bones was estimated by summing the fractions times the percentage of the skeleton for each bone involved.

A study was conducted at our institution to assess the interobserver variability of the BSI method. A series of 69 whole-body bone scans was read by 3 independent blinded observers. This was done after the 3 observers participated in a training session involving 10 images, in which they graded the images together to reach a consensus. Excluding the time spent for the training session, evaluation of each patient in this group took an average of 13.5 min per reader (Imbriaco M, Yeung H, Larson SM, personal communication, 1996). The results of this study demonstrated that when the bone involvement is less than 20% of the total skeleton, the interobserver variability is less than 10%. The variability, however, can differ by 15% for greater total skeletal involvement.

In this work, our motivation was to reduce the evaluation time and interobserver variability by a semiautomated computer algorithm. Using this method, one should be able to objectively: (a) segment metastatic bone regions from a user (physician)-selected initial seed, (b) measure the fraction of metastatic tumor involvement of each individual bone and (c) estimate the total tumor burden (mass) of the metastatic disease in a shorter time than the current BSI method.

MATERIALS AND METHODS

Image Segmentation

Region growing is an image processing procedure that groups pixels into larger regions (14). The algorithm starts with a user defined "seed" pixel and grows into regions by appending to the seed pixel, neighboring pixels that have similar gray levels. In brief:

$$PC = (x + i, y + j)$$

$$= \{1 \text{ if } ([G_s(x, y) - G_n(x + i, y + j)] <= T(c) \times G_s(x, y))$$

$$0 \text{ if } ([G_s(x, y) - G_n(x + i, y + j)] > T(c) \times G_s(x, y))$$

$$i = -1, 0, +1; \quad j = -1, 0, +1\}, \quad \text{Eq. 1}$$

where

$G_s(x, y)$: gray level of the seed pixel at x, y,
$G_n(x + i, y + j)$: gray levels of the neighbor pixels,
$T(c)$: contrast-dependent optimal threshold,
$PC(x + i, y + j)$: pixel connectivity of the neighbor pixels.

Determination of Stopping Thresholds by Phantom Experiments

The optimal threshold, $T(c)$, for cessation of the region-growing process is a function of the activity concentration ratio between the BMet and the background. To determine this optimum stopping threshold, we conducted a series of phantom studies to simulate BMets. In this experiment, an abdominal Jaszcsak phantom was used. To simulate BMets, two spheres with volumes of 4 ml and 21 ml, and an ellipsoid with a volume of 7.4 ml, were injected with a 1 μCi/ml of ^{99m}Tc and placed at various locations in the phantom. Target-to-background activity concentration ratio was changed from infinite (no background activity) to 3 by adding ^{99m}Tc into the background.

An ADAC Genesys SPECT system equipped with a low-energy high-resolution collimator was used in planar mode for data acquisition. A 20% window was centered at 140 keV and the data acquired in a 128 × 128 × 16 bit pixel matrix for 15 min. The images were transferred to a Silicon Graphics 4D/240GTX (25 MHz) workstation for region-of-interest (ROI) analysis. The optimal stopping thresholds were computed for each contrast level and fitted into a linear curve through regression.

Measurement of the Fractional Metastatic Tumor Involvement

To individualize the size or the mass of each bone for patients with metastatic tumor, we created look-up-tables (LUTs) based on measurements of individual bones given by Merz et al. (15). In that study, a series of 204 skeletons from the Terry Collection was used: American whites and blacks of both sexes between the ages of 16 and 91. The Terry Collection data were used to determine the mass of the skeleton by using seven independent variables: age, height, femur-length, area of midfemur, femur-mass, area of compact bone in femur by radiograph and measurement. For retrospective patient analysis, however, some of these independent variables are not readily available. Therefore, we performed multivariate linear regression to estimate skeletal masses of both race and sex groups using age and height variables (Table 1).

We then performed ROI analysis for every visible bone on normal anterior and posterior scans. In this way, the projected area of the individual bones was determined in terms of pixels. The total projected areas were used to normalize the area of metastatic involvement, such that:

$$F_{MiX} = A_{MiX}/A_{BiX}, \qquad \text{Eq. 2}$$

where

F_{MiX}: Fraction of metastatic involvement of ith bone in Patient X,
A_{MiX}: Area of the metastases in ith bone of Patient X (pixels),
A_{BiX}: Area of the ith bone of Patient X (pixels) in which

$$A_{BiX} = (P_{WX}/P_{WN}) \times A_{BiN}. \qquad \text{Eq. 3}$$

P_{WX}: Skeletal mass of Patient X (g),
P_{WN}: Skeletal mass of a patient with a normal bone scan (g),
A_{BiN}: Area of the ith bone of a patient with a normal bone scan (pixels).

Equation 3 states an important assumption, namely, that the area of each skeletal bone scales linearly with total skeletal mass. After the computations of each F_{MiX} for Patient X, those fractions can be converted to absolute masses using:

$$W_{MiX} = F_{MiX} \times (W_{Pi}/100) \times P_{WX}, \qquad \text{Eq. 4}$$

where

W_{MiX}: Percent mass of the ith metastases in Patient X (g),
W_{Pi}: Percent mass of the ith bone (total skeleton = 100%),
P_{WX} was computed using age and height correlated regression analysis as described in this section. To find the total mass of the metastatic lesions (W_{MX}), all W_{MiX} values are added together.

Regression Analysis

The images obtained from phantom experiments with two spheres and one ellipsoid were analyzed by the region growing algorithm (Eq. 1) initiated by the selection of a seed pixel into the spheres and ellipsoid. Connectivity of pixels surrounding the seed pixel were determined by Equation 1. Optimum region stopping thresholds [T(c)] have been adaptively determined for each volume-object/background activity concentration ratio to minimize the difference between the actual object area of the central slice and measured (by region-growing) object area. A correlation (r = 0.92) between contrast (the gray level difference between object and background regions divided by the object gray level and multiplied by 100 to express as a percentage) and T(c) was found as

$$T(c) = 0.82 \times \text{Contrast}(\%)/100 \quad \text{if Contrast} <= 75\%$$
$$T(c) = 0.4 \qquad\qquad\qquad\quad \text{if Contrast} > 75\%. \qquad \text{Eq. 5}$$

Skeletal Mass Computation

Linear equations were obtained by multivariate linear regression of skeletal mass, age and height data from Merz et al. (15) data (Table 1) using the IDL Version 4.0 program. Linear equations were used to generate LUTs and were in the form of

$$\text{Skeletal Weight (g)} = C_0 + C_1 \times \text{Age (yr)} + C_2$$
$$\times \text{Height (cm)}. \qquad \text{Eq. 6}$$

The fit parameters for each race and sex group were given in Table 2.

To tie the projected bone areas from a bone scan to actual individual bone masses, it was necessary to carefully outline all the bone structures for a reference man of known height, sex, age and race. This reference patient was a 71-yr-old white man 174 cm in height with a normal (a scintigraphic study not showing pathological areas of increased radiotracer uptake) bone scan. We estimated 4437.4 g of skeletal mass using our regression analysis. The pixel

TABLE 1
Terry Collection Data

No. of cases	Age interval (yr)	Age (yr) mean ± s.d.	Height (cm) mean ± s.d.	Skeletal weight mean ± s.d.
Black female				
12	16–29	22.2 ± 3.9	161.6 ± 8.4	3736 ± 487
7	30–39	35.7 ± 3.5	162.1 ± 8.1	4030 ± 790
8	40–49	44.5 ± 2.6	164.4 ± 6.9	3920 ± 646
8	50–59	54.8 ± 3.3	160.0 ± 3.5	3388 ± 443
6	60–69	63.8 ± 2.2	158.8 ± 3.5	3827 ± 656
9	70–79	73.0 ± 3.1	160.0 ± 5.6	3373 ± 634
5	80–91	83.8 ± 4.5	158.4 ± 7.5	3268 ± 628
White female				
7	17–39	30.0 ± 6.2	163.3 ± 5.0	3197 ± 543
4	40–49	46.5 ± 1.7	161.2 ± 7.8	3002 ± 844
7	50–59	55.0 ± 2.1	164.6 ± 5.8	3320 ± 507
8	60–69	65.0 ± 2.9	158.1 ± 7.4	2984 ± 400
8	70–79	73.0 ± 2.7	161.4 ± 7.8	3022 ± 709
5	80–89	86.4 ± 3.4	153.6 ± 8.3	2182 ± 400
Black male				
8	18–29	24.1 ± 4.3	174.9 ± 7.0	4915 ± 715
8	30–39	34.2 ± 2.9	178.5 ± 4.4	5621 ± 675
9	40–49	45.7 ± 2.8	170.6 ± 8.4	4882 ± 1009
8	50–59	56.2 ± 2.3	171.4 ± 5.6	4976 ± 890
8	60–69	62.8 ± 3.5	167.9 ± 10.2	4988 ± 480
8	70–79	73.6 ± 3.5	172.8 ± 10.4	5340 ± 946
5	80–91	86.4 ± 4.2	167.8 ± 6.4	4611 ± 832
White male				
4	18–29	21.5 ± 4.4	172.0 ± 12.3	4445 ± 999
8	30–39	35.1 ± 3.4	173.1 ± 10.5	4245 ± 624
9	40–49	44.9 ± 3.0	173.0 ± 7.0	4860 ± 710
9	50–59	55.8 ± 4.0	171.7 ± 4.7	4369 ± 569
9	60–69	66.2 ± 2.3	172.1 ± 4.9	4432 ± 701
8	70–79	73.6 ± 3.3	168.1 ± 2.8	4575 ± 349
8	80–87	82.9 ± 2.5	168.9 ± 7.5	3955 ± 457

Data were modified from Reference 16.

areas of all the bones were delineated on the anterior and posterior bone scan images. Bone pixel-area values found by ROI analysis were stored in a LUT table. These pixel areas were then used to normalize the individual patient bones with metastatic disease. Each normalized disease area was then multiplied with the fractional mass of that particular bone obtained from ICRP Publication 23 (*13*). Because the individual skeleton mass was estimated by regression analysis from the patient body mass, height, sex and race, it was then possible to compute the mass of each metastatic lesion.

A schematic diagram of the bone metastases analysis is illustrated in Figure 1. The user enters the patient's age, height, sex and race into the BMets analysis program. Using the linear regression parameters given in Table 2, the total skeletal mass of the patient is computed. Seed points are entered within each lesion by a mouse click in anterior or posterior whole-body scan of the patient. If the same lesion is visible on both scans, the scan with a higher lesion contrast is selected to introduce the seed pixel. The algorithm then applies region growing, calculates the number of pixels in each region, adjusts those regions with the reference scan pixel values (from a patient with no bone disease). Those normalized values are multiplied with bone fractions obtained from ICRP 23 (*13*). Fractional values are then multiplied with total skeletal mass of the patient to obtain the mass of each lesion.

Adaptive contrast normalization was applied if the lesion/background activity concentration ratio is equal to or less than 4 (assume lesion = 100 counts per pixel, background = 25 counts per pixel, then Contrast = (100 − 25)/100 = 0.75 or 75%). In that case, the optimal threshold was selected based on the relation given in Equation 5. However, when the activity concentration ratio is greater than 4, then the optimal threshold converges to a fixed value of 0.4.

RESULTS

To determine the fraction of metastatic involvement in each bone and to calculate the mass of bone disease, we performed a BMets analysis for 11 bone scans from 6 patients (mean age = 66). Figure 2 shows the delineation of all metastatic regions for the anterior image of Patient 1. A similar analysis was performed on both anterior and posterior images for the rest of the patients. The results of this analysis are summarized in Table 3. The percent of bone lesion involvement in the 11 scans studied ranged from 2.4% to 6.5% by the BMets analysis method as compared with 3.1% to 14.0% by the BSI approach. The BMets analysis took between 1 and 4 min for each patient

TABLE 2
Fit Parameters and Correlation Coefficient (r) for Black Female, Black Male, White Female and White Male

Race/Gender	C_0	C_1	C_2	r
Black female	−3863.8	−6.3	48.9	0.74
Black male	−8696.8	2.2	78.6	0.62
White female	−12299.3	−0.7	95.2	0.98
White male	262.3	−2.4	25.0	0.57
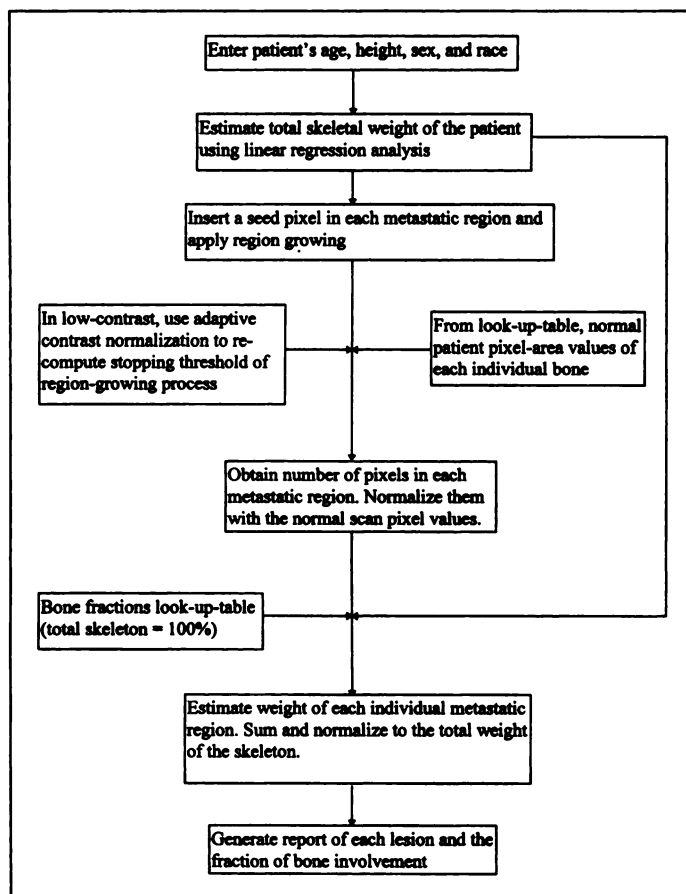
**FIGURE 1.** Overall schema for quantification of metastatic bone lesions and the total disease burden.

depending on the number of lesions and the visibility of those lesions.

Due to the errors incurred by ROI drawing (or visual estimation) by the BSI method, BMets analysis is more sensitive to small changes in disease mass due to the objectivity in the region growing algorithm (Patient 4, first and second scans). Estimates of the lesion size by the BSI are greater then by the BMets method in all cases. This is due to an overestimation by the physician during the visual inspection, and not underestimation of the area by the BMets analysis program, as substantiated by phantom measurements in which the volume of the lesions are known. The BMets results are approximately one-half those obtained by BSI irrespective of lesion size. Obtaining one-half of the size with an automated method is in good agreement when using an approximately 50% threshold of the maximum gray level in clinical practice to delineate the lesions (16).

A correlation coefficient (r) of 0.83 was found between the BSI method and the BMets analysis. Furthermore, the BMets analysis estimated the mean mass of the disease (198.1 ± 67.4 g), which is not available in the BSI method, except by a crude visual estimation of the fraction of skeletal involvement multiplied by an assumed skeletal mass. A generated scan analysis report itemizes the mass of the metastatic lesions in each involved bone. An example of such a report was given in Figure 3 for Patient 1.

DISCUSSION

Manual techniques to delineate and estimate the fractional volume of metastatic bone involvement are based on the physician's experience at defining the extension of those lesions. We are concerned that the reproducibility of manually
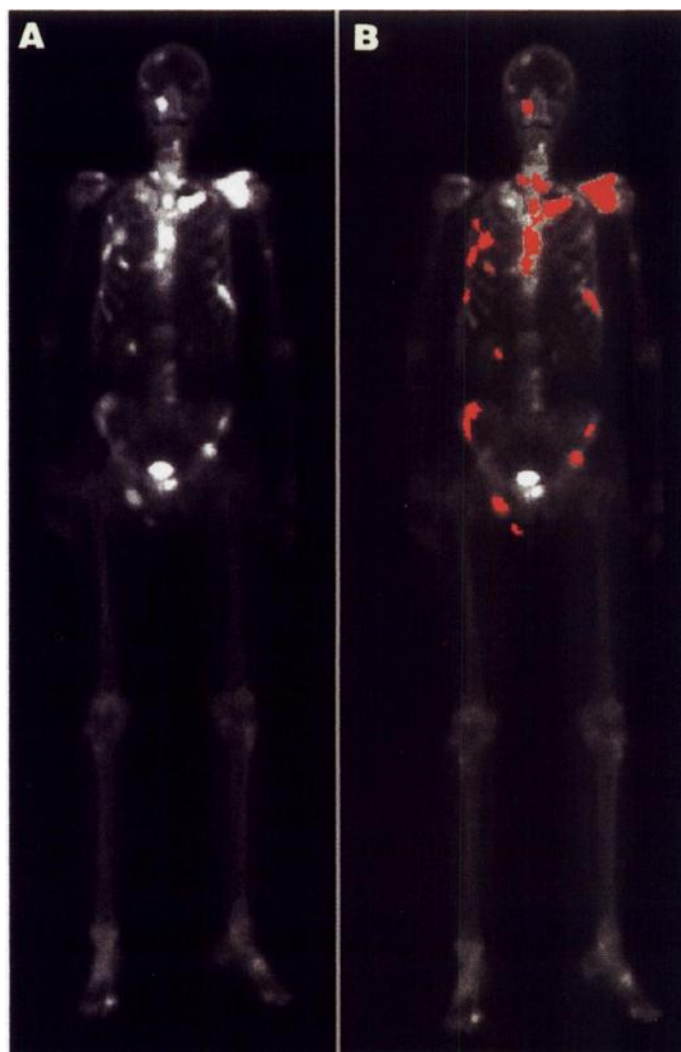
FIGURE 2. (A) Anterior bone scan of Patient 1. (B) The same image with the lesions delineated. Total delineation time for all lesions was less than 75 sec on a 25 MHz UNIX workstation.

drawn ROIs is low, especially for small lesions in areas of low contrast, due to the edge blurring of the lesion. Furthermore, since the perceived size of the lesion is a function of the display contrast, regions drawn with a fixed threshold are prone to error, especially in low lesion-to-background ratios (16). Lesions smaller than twice the full width at half maximum of the system look larger on the display, due to the limited system

TABLE 3
Bone Metastases Analysis by the BSI and BMets Methods for Six Prostate Carcinoma Patients

Patient no.	Scan date	Disease weight (g) BMets	Involvement (%) BSI	Involvement (%) BMets
1	08/17/93	109.2	8.0	2.4
2	10/28/93	227.4	10.6	5.4
3	02/01/95	127.1	3.1	2.9
4	09/23/94	123.8	5.1	2.8
	10/31/94	161.7	5.1	3.6
	12/28/94	165.1	5.4	3.7
	03/15/95	176.6	6.1	4.0
	08/21/95	256.1	9.9	5.8
5	10/26/93	273.9	11.6	5.9
	12/01/93	301.7	11.0	6.5
6	07/19/95	256.4	14.0	5.9

```
                MSKCC-NUCLEAR MEDICINE
              Report of Bone Metastasis Analysis

Patient Name: #1          MRN#: 00000000  7/10/96
Order: Dr. Larson

8/17/93 BONE SCAN:
Skeletal Weight:4597.10 gm
Radionuclide: 5.0 mCi Tc99m MDP

CLINICAL HISTORY: 67 year old male patient with prostate carcinoma is
referred for baseline study on extent of disease

PROCEDURE: Two hours post infusion anterior, posterior whole body images

FINDINGS: There is an increased uptake of Tc99m involving thoracic and lumbar
vertebrae. Increased uptake also noted in the right and left ribs, left scapula, illium,
and pubic bone.

------------------ BONE METASTASIS REGIONS ------------------
```

	Region	Area (pixels)	Percent Involvement	Disease Weight (gm)
1-	skull	61	0.88	5.75
2-	lscap	422	17.9	21.8
3-	lhumerus	33	2.12	1.84
4-	lilium	81	3.48	2.50
5-	rpubis	91	13.4	4.83
6-	RR3	66	16.2	2.87
7-	RR4	48	11.2	1.99
8-	RR7	30	6.71	1.19
9-	Sternum	316	17.1	8.08
10-	T4	54	10.0	3.07
11-	T5	42	9.27	2.12
12-	T6	49	9.69	2.24
13-	T7	51	9.71	2.93
14-	T8	46	9.54	2.67
15-	T9	42	9.27	2.12
16-	T10	38	9.04	2.02
17-	L2	52	10.3	3.19
18-	L3	58	11.4	3.56
19-	L5	68	13.4	4.18
20-	rischium	86	12.7	9.17
21-	lilium	53	2.27	1.63
22-	rilium	58	2.48	1.79
23-	LR3	83	20.3	3.61
24-	LR5	145	25.9	4.60
25-	LR6	42	7.78	1.38
26-	RR2	47	14.9	2.65
27-	RR4	86	20.1	3.56
28-	RR5	35	6.26	1.11
29-	RR12	40	18.0	1.06

```
TOTAL Regions= 29
TOTAL Disease Weight (gm)= 109.23348
TOTAL Skeletal Involvement (percent) = 2.37

IMPRESSION: Abnormal Bone Scan. Metastatic prostate cancer to bone.
```

FIGURE 3. An example of an output report generated after application of BMets to Patient 1. Some regions were delineated from the posterior image.

spatial resolution and edge blurring, which result in an overestimation of the lesion size with manual ROI methods as seen in Table 3. This finding is in good agreement with the analysis performed by Long et al. (*17*). Their results (Fig. 3A in reference *17*) show that operator-drawn ROIs significantly overestimate even large volumes up to 120 ml. Overestimation of lesion size may not be the case in BMets analysis since the adaptive threshold for region growing adopted edge information derived from phantom experiments, with known lesion size and contrast levels.

In its present state, the BMets analysis system has limitations. A preliminary work using digitized bone scan films from other medical centers with various magnification factors created a scaling problem, since the BMets algorithm was normalized by a standard patient scan with a matrix size of 512 × 1024. Therefore, the images obtained in smaller matrices require multiplication by a zoom factor with region pixels artificially changing the quantitation values. Smaller matrix sizes may reduce the accuracy of BMets and decrease the reproducibility of visual inspection or manual ROI methods.

The quantitation of digitized bone scan films was significantly less accurate than 16 bit digital camera images. In comparison with 8 bit (256 gray levels) or 16 bit (65,536 gray levels) digital data, scanned films generally demonstrate only approximately 65 gray levels. This reduced number of gray levels resulted in several erroneous connections between the background pixels into the ROIs by the semiautomated region-growing algorithm. It is also not possible to visualize all metastatic involvements in the image for seed insertion due to the limited dynamic range of the film. The quantitation of digitized films contains inaccuracies arising from two sources. First, film exhibits a nonlinear H and D response curve altering the edge gradient and interfering with the predetermined contrast-dependent threshold levels. Second, there is an inherent variability in film response, which depends on the film processor, temperature, age of the developer, etc. As a consequence, two films of the same patient bone scan can produce different results.

Another shortcoming of the BMets program is its inability to differentiate skull bones. The whole-body sweep images provide two-dimensional projections of a three-dimensional structure. The BMets program performs fractional metastatic deposit measurements on these two-dimensional data. Bones that are perpendicular to the image plane become grouped together. For example, all the bones in the skull were considered as a single bone in the program, and metastatic fractions were computed with respect to the whole skull.

The effectiveness of BMets analysis is reduced at low lesion-to-background ratios (e.g., 3) due to the increased noise at the region boundary, which interferes with the accuracy of the region growing process. To overcome this problem, we have integrated an adaptive contrast adjustment program that measures lesion-to-background ratio and adjusts the stopping threshold (see Eq. 5) of region growing according to the results of phantom measurements.

Future refinements of the BMets analysis program will consider the region growing process in combination with a statistical decision-making algorithm in which stopping thresholds are computed based on the local information density. It will also be useful in investigating prefiltering of the images to remove noise while preserving region boundaries [e.g., edge-preserving smoothing algorithm (*18*)]. Although prefiltering may alter pixel values near the edges, the absolute quantitation of the pixels is not necessary since the BMets program attempts to find the size of the area rather than actual pixel values.

CONCLUSION

A new BMets quantitation method has been developed. This method uses an adaptive contrast adjustment scheme in order to minimize the lesion delineation error, which would generally result in different lesion sizes at variable contrast levels. Two clinical goals have been achieved: (a) a reduction in the time for delineation of bone lesions by at least two times compared to BSI method and (b) increased objectivity and reproducibility in assessing the fraction of the metastatic involvement of each bone considering 15% interobserver variation with the BSI method. These advantages release the physician from laborious ROI drawing, replacing this chore by the more appropriate diagnostic task of "point and click" at lesions in the skeleton, and preserve the physicians diagnostic skills to recognize bony lesions, and combines it with an objective method to determine the lesion area (and from it the fractional mass). This objectivity

makes the technique user independent. Interphysician variability only occurs when the interpretation of the involvement of individual bones differs. Another significant advantage of this method is the analysis of repeat bone scans of the same patient after treatment. In this circumstance, the reproducibility of the region growing will give a precise result of the change in disease status, which could readily be overwhelmed by the uncertainties in the ROI drawing, even when the scans are delineated by the same physician. The assessment of bone scans in a quantitative manner will enable a more objective evaluation of therapies directed at the treatment of bone metastases. The quantitation of metastatic fractions on an individual bone basis and the generation of a treatment report (Fig. 3) that classifies the fractional involvement of each bone allows response to be determined for each lesion.

ACKNOWLEDGMENTS

REFERENCES

1. Krishanamurthy GT, Blahd WH. Technetium-99m polyphosphate bone image for early detection of skeletal metastases: correlation with other diagnostic parameters. *J Nucl Med* 1975;13:330–340.
2. Rosenthall L, Lisbona R. Skeletal imaging. In: Baum S, ed. *Current practice in nuclear medicine.* Norwalk, CT: Appleton-Century-Crofts; 1984:56.
3. Pantelides ML, Bowman SP, George NJ. Levels of prostate specific antigen that predict skeletal spread in prostate cancer. *Br J Urol* 1992;70:299–303.
4. Miller PD, Eardley I, Kirby RS. Prostate specific antigen and bone scan correlation in the staging and monitoring of patients with prostatic cancer. *Br J Urol* 1992;70:295–298.
5. Yamashita K, Denno K, Ueda T, et al. Prognostic significance of bone metastases in patients with metastatic prostate cancer. *Cancer* 1993;71:1297–1302.
6. Krishanamurthy GT, Hiss JM, Tubis M, Blahd WH. Pattern of distribution of metastatic bone disease in man [Abstract]. *J Nucl Med* 1976;17:526.
7. Bushnell DL, Browne G, Miller S, Pettit W, Kahn D. Hematologic toxicity following therapy with strontium-89 or samarium-153 EDTMP and scintigraphic extent of skeletal metastases [Abstract]. *J Nucl Med* 1996;37:31P.
8. Calderon C, Molina IL, Garcia SC. Toxic effects of strontium-89 treatment and its relation with the extension of bone metastases [Abstract]. *J Nucl Med* 1995;36:30P.
9. Soloway MS, Hardeman SW, Hickey D, et al. Stratification of patients with metastatic prostate cancer based on extent of disease on initial scan. *Cancer* 1988;61:195–202.
10. Amico S, Liehn JC, Desoize B, Larbre H, Deltour G, Valeyre J. Comparison of phosphate isoenzymes PAP and PSA with bone scan in patients with prostate carcinoma. *Clin Nucl Med* 1991;16:643–648.
11. Chybowski FM, Keller JL, Bergstralh EJ, Oesterling JE. Predicting radionuclide bone scan findings in patients with newly diagnosed untreated prostate cancer: prostate specific antigen is superior to all other clinical parameters. *J Urol* 1991;145:313–318.
12. Sabbatini P, Yeung H, Imbriaco M, et al. The correlation of serial bone scintigraphy and PSA determinations in patients (Pts) with androgen independent prostate cancer (AIPC) [Abstract]. *Proc Am Soc Clin Oncol* 1996;15:254.
13. International Commission on Radiation Protection. *Publication 23: report of the task group on reference man.* New York: Pergamon Press; 1992.
14. Gonzales RC, Wintz P. *Digital Image Processing.* Reading, MA: Addison–Wesley; 1987:369–373.
15. Merz AL, Trotter M, Peterson RR. Estimation of skeleton weight in the living. *Am J Phys Anthropol* 1956;14:589–609.
16. Erdi YE, Wessels B, Loew M, Erdi A. Threshold estimation in SPECT and planar imaging for clinical radioimmunotherapy. *Cancer Res* 1995;55(suppl):5823s–5826s.
17. Long DT, King MA, Sheehan J. Comparative evaluation of image segmentation methods for volume quantitation in SPECT. *Med Phys* 1992;19:483–489.
18. Nagao N, Matsuyama T. *A structural analysis of complex aerial photographs.* New York: Plenum Press; 1980.

FIRST IMPRESSIONS
Renal Ectopia in Bone Scanning
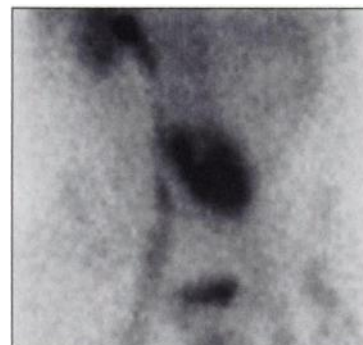

Figure 1.

Figure 2.

Figure 3.

PURPOSE

A 45-yr-old male athlete underwent bone scintigraphy for hip pain, a left femoral neck stress fracture being suspected. The intense focal uptake of ⁹⁹ᵐTc-HDP in the anterior pelvic view at the S1 level (Fig. 1) was demonstrated in the LAO view (Fig. 2) to be extra-osseous. Review of the initial blood-pool image (Fig. 3) identified the focus as residual radioactive urine in a renal calyx of his midline ectopic pelvic kidney.

TRACERS
Technetium-99m-HDP (900 MBq)

ROUTE OF ADMINISTRATION
Intravenous

TIME AFTER INJECTION
Dynamic and blood pools immediately after administration. Delayed static images at 2.5 hr.

INSTRUMENTATION
General Electric 4000 XRT

CONTRIBUTORS
Clayton J. Frater and I. Provan. C. Murray, Nuclear Diagnostics Randwick, Sydney, Australia.